The Growth and Decay of Low-Frequency Anomalies in a GCM

STEVEN FELDSTEIN

Earth System Science Center, The Pennsylvania State University, University Park, Pennsylvania

(Manuscript received 5 July 1996, in final form 18 June 1997)

ABSTRACT

The temporal evolution of a regional-scale persistent low-frequency anomaly is examined with data from a 2100-day perpetual January general circulation model. The persistent episodes are determined with an objective analysis of the low-pass (>10 day) 350-mb streamfunction field that uses both pattern correlations and empirical orthogonal function (EOF) analysis.

The composite evolution of each term in the streamfunction tendency equation is calculated relative to the onset day (the first day of the persistent episode). By projecting each term in the streamfunction tendency equation onto an EOF (the EOF is associated with a particular low-frequency anomaly), the contribution of these terms toward the tendency of the corresponding principal component can be obtained. It is found that the sum of the linear terms dominates during most of the growth and the decay of the low-frequency anomaly. The linear term that accounts for the growth and maintenance of the low-frequency anomaly is the interaction between the anomaly and the time-mean zonally asymmetric flow. After the anomaly attains sufficient amplitude, its decay is accomplished through the divergence term. For one phase of the EOF, it is found that the high-frequency transients prolong the anomaly, whereas in the other phase they do not.

Implications of this study for examining monthly averaged anomalies are also discussed.

1. Introduction

Among the broad range of timescales of midlatitude atmospheric motions, the dynamical mechanisms associated with intraseasonal variability have recently received much attention. Numerous observational studies find that these intraseasonal, or low-frequency, fluctuations take the form of a small number of recurring persistent regional anomalies (e.g., Wallace and Gutzler 1981). Most studies of midlatitude low-frequency persistent anomalies use *time averaged* diagnostics and concentrate their investigation on the maintenance of the anomalous low-frequency circulation. These studies have proposed an array of different hypotheses for maintenance, including 1) modification of the low-frequency anomaly due to wave propagation and/or instabilities of the zonally asymmetric climatological flow (e.g., Frederiksen 1983; Simmons et al. 1983; Branstator 1990, 1992), 2) linear dispersion from remote anomalous diabatic or topographic forcing (e.g., Hoskins and Karoly 1981), 3) amplification by anomalous high-frequency transient eddy forcing (e.g., Egger and Schilling 1983; Lau 1988; Branstator 1992; Ting and Lau 1993), and 4) changes in quasi-stationary eddies associated with fluctuations in the zonal mean flow (e.g., Branstator 1984; Nigam and Lindzen 1989; Kang 1990).

Most studies are restricted to an examination of anomaly maintenance and do not address the mechanisms that cause the onset and decay of the persistent anomaly, that is, its full temporal evolution. On the other hand, there have been a number of studies that find systematic temporal alterations in wave activity vectors, storm tracks, energetics, enstrophy, and tropical precipitation that accompany the evolution of low-frequency anomalies (e.g., Dole 1986; Dole and Black 1990; Nakamura and Wallace 1990; Schubert and Park 1991; Black and Dole 1993; Higgins and Schubert 1994, 1996). Nevertheless, these studies do not evaluate quantitatively which particular mechanisms are most important at different stages during the evolution of the low-frequency anomaly.

The purpose of this paper is to identify the growth and decay mechanisms of low-frequency anomalies by examining the composite temporal evolution of each term in the streamfunction tendency equation at different times during the anomaly evolution. It is important to emphasize that this approach is descriptive and cannot elucidate fundamental dynamic mechanisms. Nevertheless, as we will find, important insight can be obtained from this approach. Furthermore, as low-frequency streamfunction anomalies can be implicitly forced via the divergence term (Navarra and Miyakoda 1988), we briefly examine each term in the divergence equation. For this study, data from a perpetual January Geo-

Corresponding author address: Dr. Steven Feldstein, Earth System Science Center, The Pennsylvania State University, 248 Deike Building, University Park, PA 16802.
E-mail: sbf@essc.psu.edu

physical Fluid Dynamics Laboratory (GFDL) General Circulation Model (GCM) will be used. The primary advantage of using a GCM is simply that the streamfunction tendency budget is much better balanced than with observational data.

In section 2, a description of the model and the diagnostic techniques will be presented. The results, emphasizing the inverse Laplacian of the vorticity equation, will be shown in section 3. The conclusions will be presented in section 4.

2. Model description and diagnostic techniques

The data to be examined in the study were generated from a 2100-day perpetual January GFDL GCM run. This model has nine vertical levels, rhomboidal-30 horizontal resolution, realistic topography, and sea surface temperatures specified at their climatological January values. This model includes all the physical processes of a full GCM, including a complete radiation package, moist convective adjustment, predicted clouds, etc. A more complete description of GFDL GCMs can be found in Gordon and Stern (1982). All data generated by this model are saved daily on sigma surfaces. However, to compare results with those from other studies, logarithmic interpolation from sigma to pressure coordinates is performed.

In this study, we examine the composite temporal evolution of a 350-mb low-frequency streamfunction anomaly. We use an objective definition for each persistent episode, adopted from Horel (1985) and Mo (1986), which is based on the pattern correlation r at day t and lag τ defined as

$$r(t, \tau) = \frac{\langle \psi'(\lambda, \theta, t)\psi'(\lambda, \theta, t + \tau)\rangle}{\sigma[\psi'(\lambda, \theta, t)]\sigma[\psi'(\lambda, \theta, t + \tau)]}, \quad (1)$$

where $\psi(\lambda, \theta, t)$ is the deviation of the 350-mb streamfunction from its corresponding time mean at that grid point, $\psi' = \psi(\lambda, \theta, t) - \langle\psi(\lambda, \phi, t)\rangle$, $\sigma^2[\psi'(\lambda, \theta, t)] = \langle(\psi'(\lambda, \theta, t))^2\rangle$, the angle brackets denote a horizontal average over the Northern Hemisphere, and λ and θ are the longitude and latitude respectively. If the pattern correlations $r(t, \tau)$ and $r(t + 1, \tau)$ exceed a particular threshold value for five or more consecutive days, that is, if $r(t, \tau)$ and $r(t + 1, \tau) \geq r_c$, for $\tau = 1$ to 5, a persistent episode is defined to have taken place. In this study, $r_c = 0.42$, which corresponds to the 97.5% significance level. The number of degrees of freedom, required for this calculation, can be obtained from the Fisher Z-transformation (also see Feldstein and Lee 1996) of the pattern correlations. Once a persistent episode is determined, an onset day is defined to correspond to the first day of the persistent episode.

There are two additional requirements that are used to classify persistent episodes. These are that the magnitude of the principal component (expansion coefficient) of a particular EOF (empirical orthogonal function) 1) exceeds one standard deviation on the onset day and 2) is larger than that of each of the other EOFs. Also, when the principal component is positive (negative) during the onset day, we refer to those episodes as corresponding to the positive (negative) phase. Furthermore, if the last day in a persistent episode occurs within 15 days of the onset day for the next episode and if these two episodes are of the same phase, then the latter episode is discarded and is regarded as being part of the former episode.

In this study, a 31 point low-pass (>10 days) digital filter is applied to the streamfunction field. Because several studies have found that the growth or decay of various low-frequency anomalies may be as brief as 5 days (Dole 1986; Yang and Reinhold 1991; Hansen and Sutera 1995), it is important to assess the influence of this filter by comparing the results with those obtained from unfiltered data. When this comparison is made, it is indeed found that the differences between the results with and without the filter are very small. This will be discussed in more detail in the next section. Furthermore, as different flux terms are needed to complete the analysis of the streamfunction tendency budget, a high-pass (<10 days) filter of various quantities is also required. Although this 10-day cutoff for separating low and high frequency is to some extent arbitrary (a wavenumber–frequency spectrum for 350-mb streamfunction yielded no gap in the model's power spectrum), this filter does yield the distinct structural differences between high- and low-frequency eddies found in observational data (Hoskins et al. 1983).

3. Results

a. EOF analysis and persistent episodes

As stated in the previous section, the categorization of persistent episodes requires that an EOF analysis of the entire Northern Hemisphere 350-mb low-frequency, streamfunction field be performed (Figs. 1a and 1b). The first two EOFs (EOF1 and EOF2, hereafter) of the 350-mb streamfunction field constitute 14% and 10% of the total variance, respectively. (An EOF analysis of the unfiltered streamfunction field yielded almost identical spatial patterns with a decrease in variance of approximately 2% for both EOF1 and EOF2.) A calculation of the standard errors of EOF1 and EOF2 (not shown) verifies that these two EOFs are distinct (North et al. 1982). As is typically found when examining upper-tropospheric global streamfunction EOFs (Branstator 1990; Kang and Lau 1994), the first EOF is characterized by a predominantly zonally symmetric pattern in the Tropics. Kang and Lau (1994) show that this pattern corresponds to extrema in the observed globally integrated relative angular momentum. As can be seen in Fig. 1, EOF1 is indeed mainly zonal throughout much of the Tropics but also includes a large amplitude signal in midlatitudes. In contrast, EOF2 is much more regional in scale, as it resembles a wave train dominated

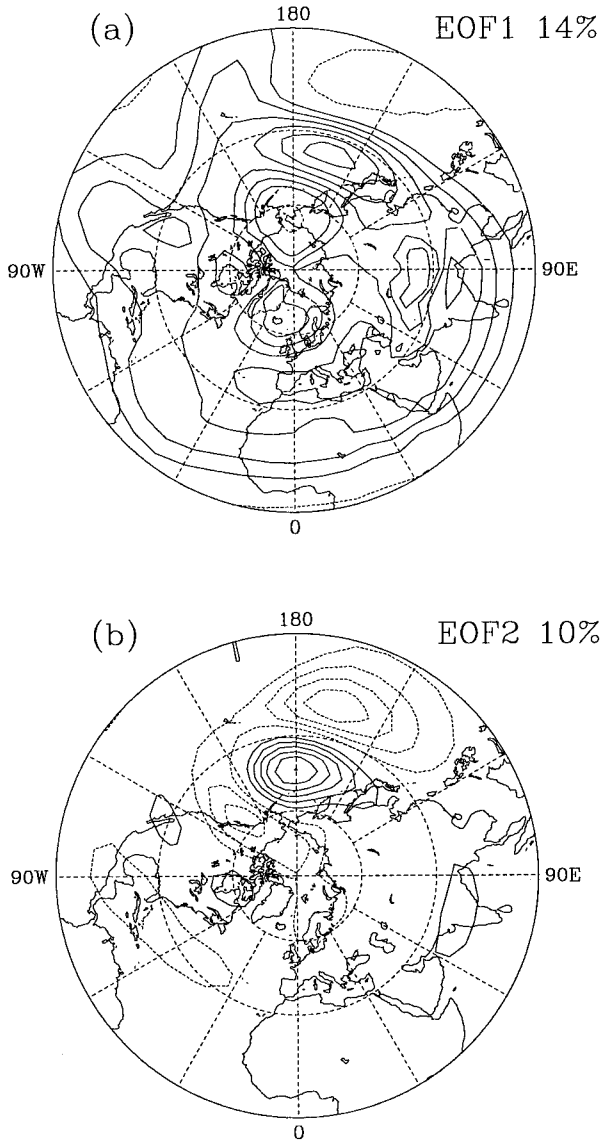

FIG. 1. Low-pass filtered 350-mb streamfunction (a) EOF1 and (b) EOF2. Contour interval is 0.15 in (a) and 0.30 in (b). Solid contours are positive, dashed contours negative, and the zero contour is omitted.

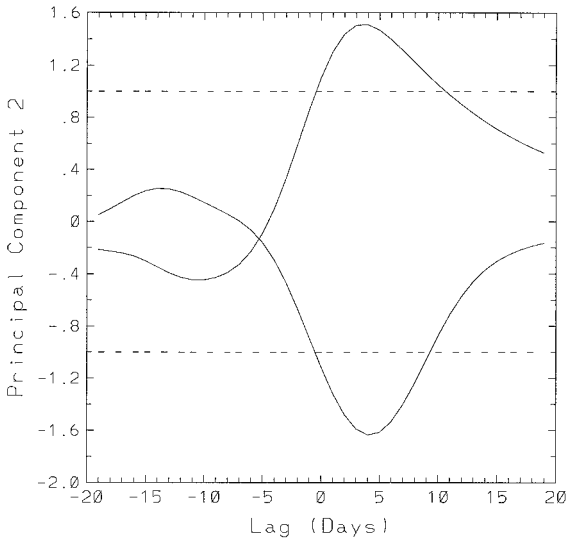

FIG. 2. Lag composites of the EOF2 principal component relative to the onset day (lag 0) for the positive and negative phases. The straight dashed lines indicate the one standard deviation level.

by a dipole in the northwest Pacific. This pattern bears some resemblance to anomalies observed in the atmosphere, such as the Western Pacific pattern in Wallace and Gutzler (1981) and the west Pacific oscillation in Barnston and Livezey (1988), both exhibiting dipoles in the northwest Pacific. As the primary aim of this study lies with regional midlatitude anomalies, for the remainder of this study, only the results for EOF2 will be presented.

It was found that there were 21 persistent episodes for both the positive and the negative phase. The length of time for a persistent episode can be determined by examining composites of the corresponding principal component. This is shown for EOF2 in Fig. 2, where it can be seen that the amplitude of the composite principal component for the positive (negative) phase remains above one standard deviation for approximately 11 (10) days. If instead, one is to define the length of a persistent episode as that for which the principal component exceeds 0.5 standard deviations, then the persistent episode lasts for more than 23 (15) days for the positive (negative) phase. A similar analysis with the unfiltered streamfunction field finds a composite principal component time series that is almost identical to that shown in Fig. 2, with the only noticeable differences being that the filtered composite time series is slightly smoother. Thus, the application of the low-pass filter has essentially no influence on either the composite growth and decay rate or the length of the persistence episode. Also, it is important to note that compositing based on the onset day (lag 0) selectively favors rapid growth on that day. This property is reflected for both phases in Fig. 2, which give the impression that the growth of the anomaly is more rapid than its decay. [The growth and decay characteristics for anomalies composited in this manner are discussed in detail in Feldstein and Lee (1996).]

b. Streamfunction anomaly evolution

We next examine the temporal evolution for the positive phase of the composite low-frequency anomalous 350-mb streamfunction (see Fig. 3). This is performed for different lags relative to the onset day. Prior to onset (lags -8 and -4), weak anomalies can be seen downstream of where the persistent anomaly will form. These anomalies propagate slowly westward and then rapidly grow while in a fixed position over the northwest Pacific

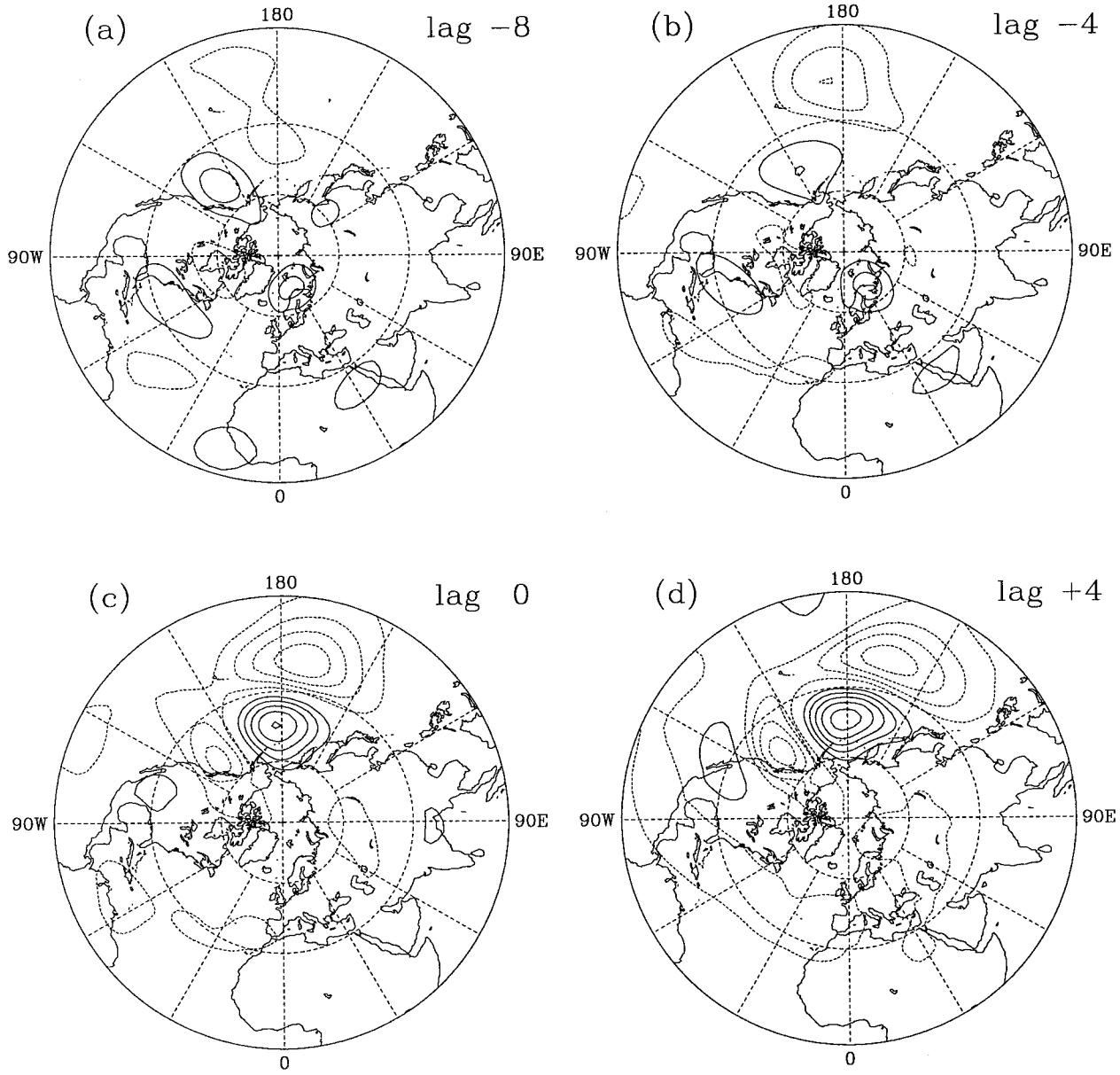

FIG. 3. Composites of the anomalous low-pass filtered 350-mb streamfunction at (a) lag −8 days, (b) lag −4 days, (c) lag 0, (d) lag +4 days,

Ocean. The structure of the anomaly closely resembles EOF2 by lag 0, reaches its largest amplitude at lag +4, and then slowly decays through lag +12 and beyond. This pattern for the growth and decay of the anomaly is of course what one would have expected from Fig. 2. Furthermore, there is also evidence of some dispersion downstream toward North America. Similar properties, but of opposite sign, are found for the negative phase. In addition, the sensitivity to the filtering procedure was further evaluated by examining the composite evolution of the unfiltered streamfunction anomalies. For this calculation, no filtering was used in both the EOF analysis and the determination of the onset days. Nevertheless, almost identical patterns to those shown in Fig. 3 were obtained.

c. Streamfunction tendency equation

Following the procedure used by Cai and Van den Dool (1994), the low-frequency streamfunction tendency equation can be written as

$$\frac{\partial \psi^L}{\partial t} = \sum_{i=1}^{8} \xi_i + R, \tag{2}$$

where

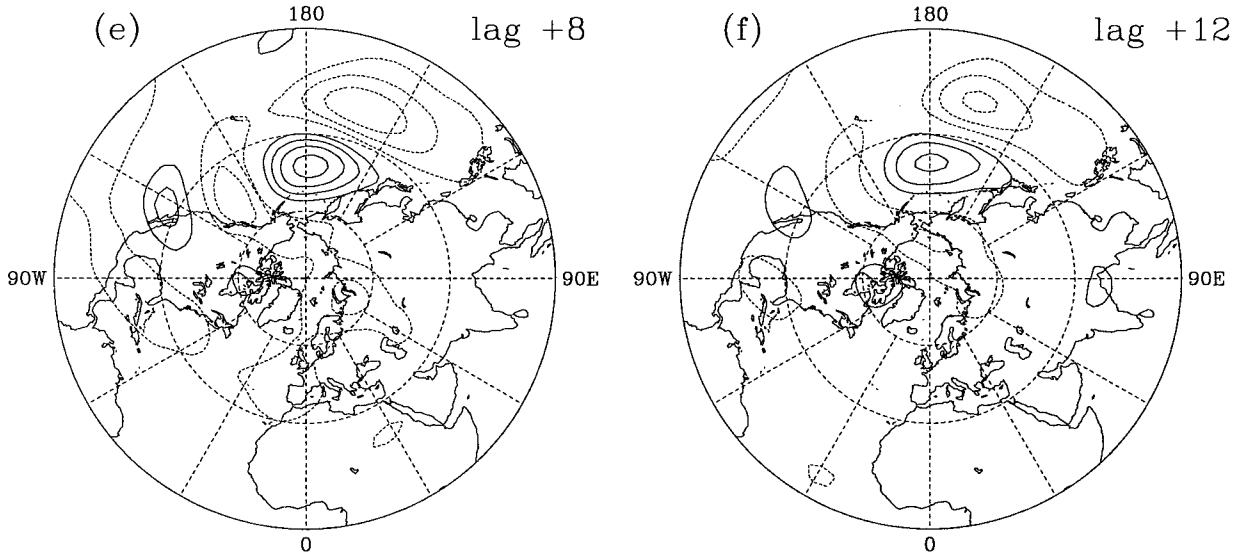

FIG. 3. (*Continued*) (e) lag +8 days, and (f) lag +12 days. Contour interval is 3×10^6 m^2 s^{-1}. Solid contours are positive, dashed contours negative, and the zero contour is omitted.

$$\xi_1 = \nabla^{-2}\left(-\left(v_r^L + v_d^L\right)\frac{1}{a}\frac{df}{d\theta}\right)$$

$$\xi_2 = \nabla^{-2}(-[\overline{\mathbf{v}_r}]\cdot\nabla\zeta^L - \mathbf{v}_r^L\cdot\nabla[\overline{\zeta}]) + \nabla^{-2}(-[\overline{\mathbf{v}_d}]\cdot\nabla\zeta^L - \mathbf{v}_d^L\cdot\nabla[\overline{\zeta}])$$

$$\xi_3 = \nabla^{-2}(-[\overline{\mathbf{v}_r^*}]\cdot\nabla\zeta^L - \mathbf{v}_r^L\cdot\nabla\overline{\zeta^*}) + \nabla^{-2}(-[\overline{\mathbf{v}_d^*}]\cdot\nabla\zeta^L - \mathbf{v}_d^L\cdot\nabla\overline{\zeta^*})$$

$$\xi_4 = \nabla^{-2}(-(f + \overline{\zeta})\nabla\cdot\mathbf{v}_d^L - \zeta^L\nabla\cdot\overline{\mathbf{v}_d})$$

$$\xi_5 = \nabla^{-2}(-\mathbf{v}_r^L\cdot\nabla\zeta^L)^L + \nabla^{-2}(-\nabla\cdot(\mathbf{v}_d^L\zeta^L))^L$$

$$\xi_6 = \nabla^{-2}(-\mathbf{v}_r^H\cdot\nabla\zeta^H)^L + \nabla^{-2}(-\nabla\cdot(\mathbf{v}_d^H\zeta^H))^L$$

$$\xi_7 = \nabla^{-2}(-\mathbf{v}_r^L\cdot\nabla\zeta^H)^L + \nabla^{-2}(-\nabla\cdot(\mathbf{v}_d^L\zeta^H))^L + \nabla^{-2}(-\mathbf{v}_r^H\cdot\nabla\zeta^L)^L\ \nabla^{-2}(-\nabla\cdot(\mathbf{v}_d^H\zeta^L))^L$$

$$\xi_8 = \nabla^{-2}(-\mathbf{k}\cdot\nabla X(\omega^L\partial\overline{\mathbf{v}}/\partial p)) + \nabla^{-2}(-\mathbf{k}\cdot\nabla X(\overline{\omega}\partial\mathbf{v}^L/\partial p)) + \nabla^{-2}(-\mathbf{k}\cdot\nabla X(\omega'\partial\mathbf{v}'/\partial p))^L,$$

and ψ is streamfunction, ζ relative vorticity, $\mathbf{v}$ horizontal wind vector, v meridional wind component, ω vertical wind component, a the earth's radius, and f the Coriolis parameter. The term R represents a residual. The subscripts "r" and "d" indicate the rotational and divergent components of the horizontal wind, respectively, and the superscripts "L" and "H" represent low-pass and high-pass filtered quantities, respectively. For low-pass filtered quantities, the (2100 day) time mean is also subtracted. An overbar denotes a time mean, prime a deviation from the time mean, square brackets a zonal average, and an asterisk a deviation from the zonal average. All other quantities have standard meteorological definitions. The term $\partial\psi^L/\partial t$ is evaluated using centered time differencing.

The interpretation of each ξ_i is as follows: ξ_1 represents planetary vorticity advection by the low-frequency flow, ξ_2 (ξ_3) the interaction between the zonal mean (zonally asymmetric) time-mean flow and the low-frequency component of the flow, ξ_4 the low-frequency contribution to the divergence term, ξ_5 (ξ_6) the self-interaction among the low (high) frequency transient eddies, ξ_7 the interaction between the low- and high-frequency transient eddies, and ξ_8 the sum of the vertical vorticity advection and tilting terms.

The extent to which the budget for the positive phase is balanced is shown in Fig. 4a where contours of the rhs (right-hand side) of (2), excluding R, overlay shading of the lhs (left-hand side) of (2) at lag -2 days, the time when the tendency of the principal component is at its largest value. As can be seen, there is an excellent match in the pattern of the two fields at most locations. However, it is important to note that even with a GCM, due to sampling errors, it is impossible to obtain a perfectly balanced budget. These errors arise because the data are saved daily and not at every time step. Additional errors result from the linear interpolation procedure and the exclusion of the linear diffusion term in (2). However, after application of the inverse Laplacian operator, the contribution from the linear diffusion term is negligible. The error in this budget, represented by R in (2), is shown in Fig. 4b (a comparable magnitude for R is also found for the negative phase). Clearly, the magnitude of R is substantially smaller than the sum of the other terms on the rhs of (2). Most importantly, the magnitude of R is substantially smaller than that found in observations.

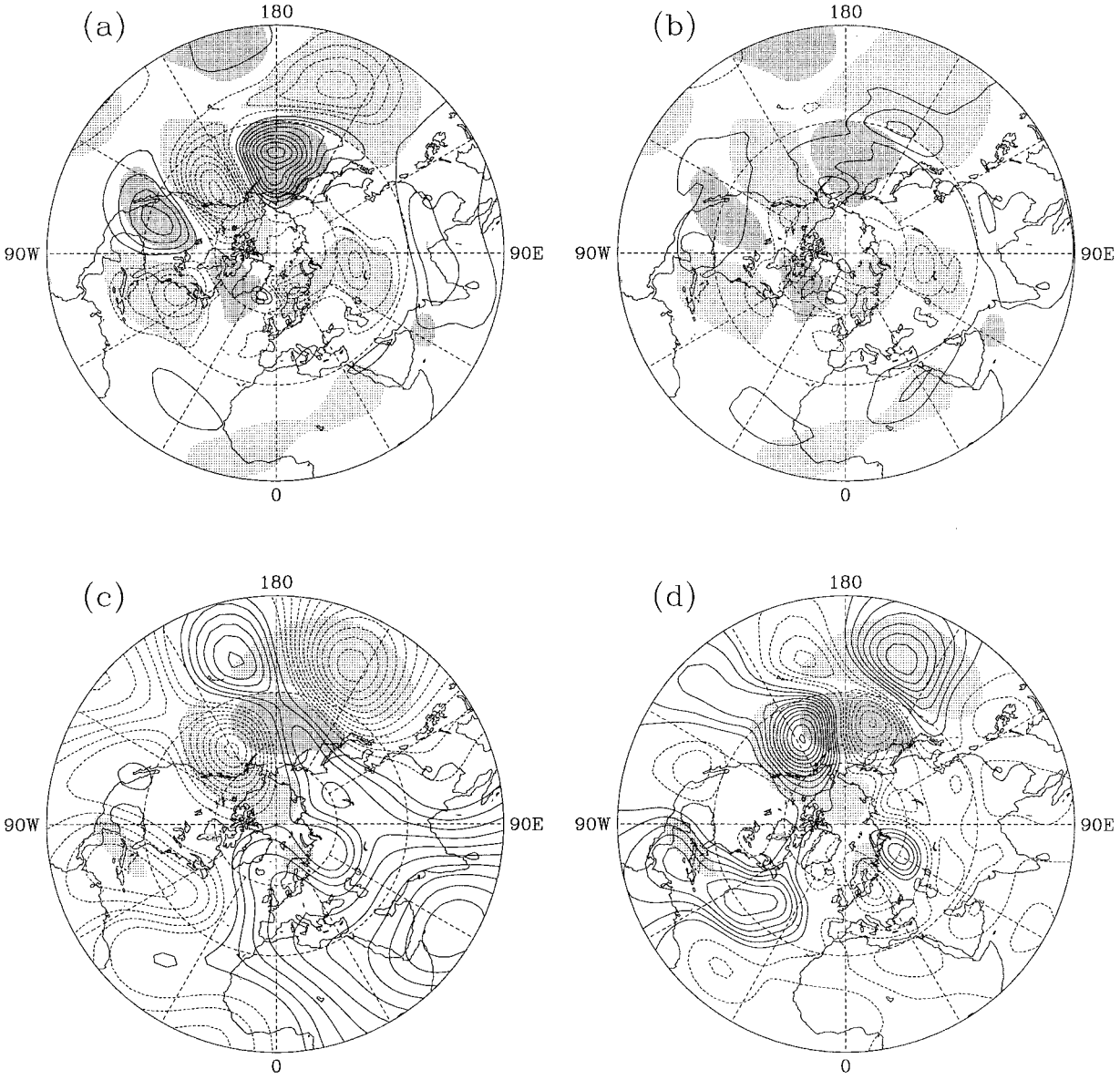

FIG. 4. Composites at lag −2 days of various combinations of terms on the rhs of (2): (a) the sum of all terms of the rhs of (2), $\Sigma_{i=1}^{8} \xi_i$, (b) the residual R, (c) ξ_1, (d) ξ_2, (e) ξ_3, (f) ξ_4, (g) the sum of the four linear terms of the rhs of (2), $\Sigma_{i=1}^{4} \xi_i$, and (h) the low-frequency

For example, in the observational study of Cai and Van den Dool (1994), who examined (2) for planetary waves, it was found that even though the pattern of the rhs and lhs of (2) were similar, the magnitude of R was almost the same as that of the lhs of (2).

Figures 4c–h show maps of various combinations of terms on the rhs of (2), along with EOF2, which is denoted by shading. Each of these maps corresponds to the positive phase at lag −2 days, that is, the time when the principal component is increasing most rapidly. Figures 4c–f show the linear terms ξ_i, $i = 1, 4$. As expected, ξ_1 (ξ_2) (see Figs. 4c, 4d) is associated with westward (eastward) propagation of the anomaly, and there is large cancelation between these two terms. The term ξ_3 (Fig. 4e), as described in the introduction, is associated with wave propagation and/or instability in a zonally asymmetric flow [instability of the zonally asymmetric flow, as in Simmons et al. (1983), involves ξ_1 and ξ_2, in addition to ξ_3, but a positive projection of ξ_3 onto EOF2 is necessary for such an instability to take place]. Inspection of Fig. 4e reveals a positive projection onto EOF2, indicating that at lag −2 days this term does contribute toward the amplification of the anomaly. The divergence term ξ_4 (Fig. 4f) is associated with westward

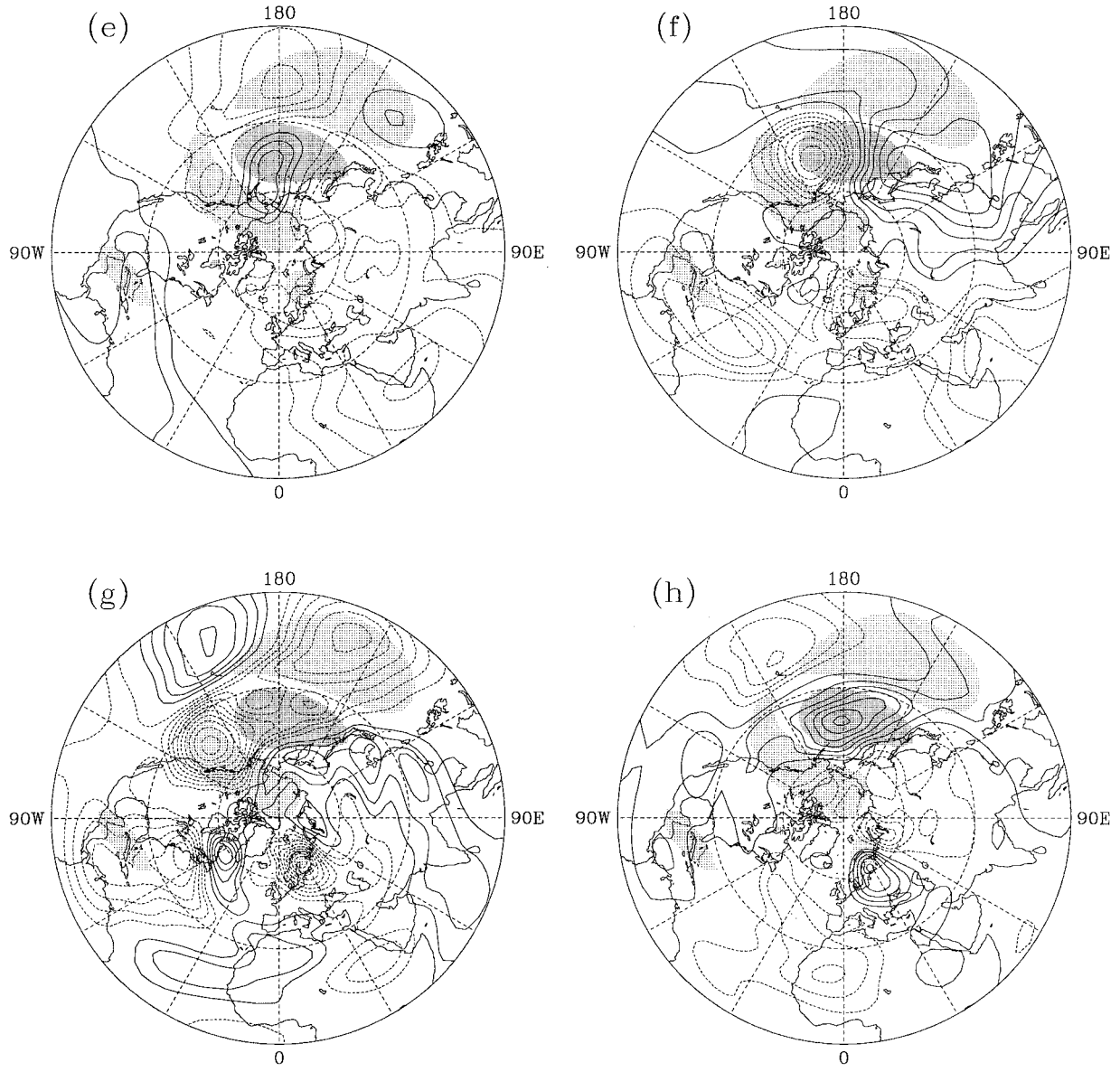

FIG. 4. (*Continued*) interaction term ξ_5. Contour interval is 5.0 $m^2\ s^{-2}$ in (a) and (b), 10.0 $m^2\ s^{-2}$ in (c) through (f), and 5.0 $m^2\ s^{-2}$ in (g) and (h). Solid contours are positive, dashed contours negative, and the zero contour is omitted. Dense (light) stippling indicates positive (negative) values of the anomalous low-pass filtered 350-mb streamfunction tendency in (a) and (b) and EOF2 in (c) through (h). The stippling is above a magnitude of 5.0 $m^2\ s^{-2}$ in (a) and (b), and above 0.40 in (c) through (h).

movement of the anomaly. When these four linear terms are summed (Fig. 4g), substantial cancelation occurs (note that the contour interval in Fig. 4g is half that in Figs. 4c–f). It is presumably because of this cancelation that the observational studies fail to achieve a well-balanced streamfunction tendency budget (Cai and Van den Dool 1994). As can be seen, there is a particularly strong projection of the sum of the linear terms onto EOF2 where EOF2 is negative.

The amplitude of the low-frequency interaction term, ξ_5 (see Fig. 4h; the same contour interval as in Fig. 4g is used), is about half that of the sum of the four linear terms. In addition, ξ_5 does appear to project positively onto EOF2, particularly where EOF2 is positive. The high-frequency ''forcing'' term at lag -2 days, ξ_6 (see Fig. 6b; the same contour interval as in Figs. 4g, and h is used), is substantially smaller in amplitude than each of the terms discussed above. However, ξ_6 does project onto EOF2, where it is positive. The remaining terms in (2), ξ_7 and ξ_8, are not illustrated. The high/low transient interaction terms ξ_7 are substantially smaller than ξ_6. The tilting plus vertical vorticity advection term ξ_8 is about one-third the magnitude of ξ_6 and lacks any coherent organization.

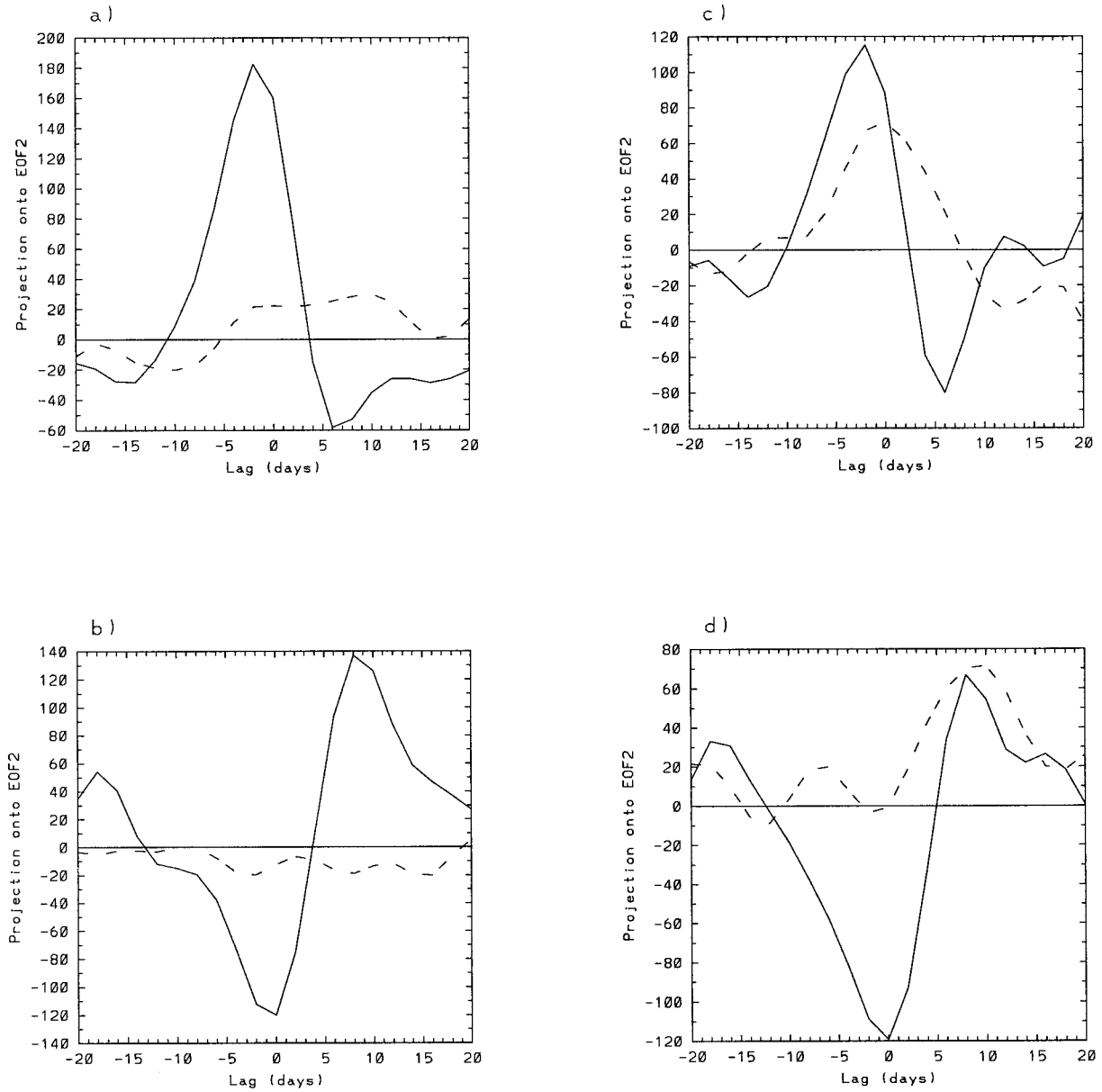

FIG. 5. Lagged projections of various combinations of terms on the rhs of (2) onto EOF2. The terms being projected onto EOF2 are (a) positive phase, solid line $\Sigma_{i=1}^{5}\,\xi_i$, dashed line ξ_6; (b) negative phase, solid line $\Sigma_{i=1}^{5}\,\xi_i$, dashed line ξ_6; (c) positive phase, solid line $\Sigma_{i=1}^{4}\,\xi_i$, dashed line ξ_5; (d) negative phase, solid line $\Sigma_{i=1}^{4}\,\xi_i$, dashed line ξ_5; (e) positive phase, solid line ξ_3, dashed line $\xi_1 + \xi_2 + \xi_4$; (f) nega-

d. Projections onto EOF2

A concise method for examining the temporal evolution of either phase of EOF2 is to project combinations of terms on the rhs of (2) onto EOF2. We examine the impact of this projection by first noting that the streamfunction can be written as

$$\psi^L = \sum_{n=1}^{N} a_n(t)E_n(\lambda,\ \theta), \tag{3}$$

where a_n and E_n are the principal components and EOFs, respectively. Substitution of this expression for ψ^L into (2), together with neglecting of R, yields

$$\sum_{n=1}^{N} \frac{da_n}{dt}E_n = \sum_{i=1}^{8} \xi_i. \tag{4}$$

Using the property that the $E_n \cos^{1/2}\theta$ form an orthonormal set of basis functions [the metric factor $\cos^{1/2}\theta$ arises from the reduction in unit area with increasing latitude (North et al. 1982)], multiplication of both sides of (4) by $E_2 \cos(\theta)$, where E_2 denotes EOF2, and sum-

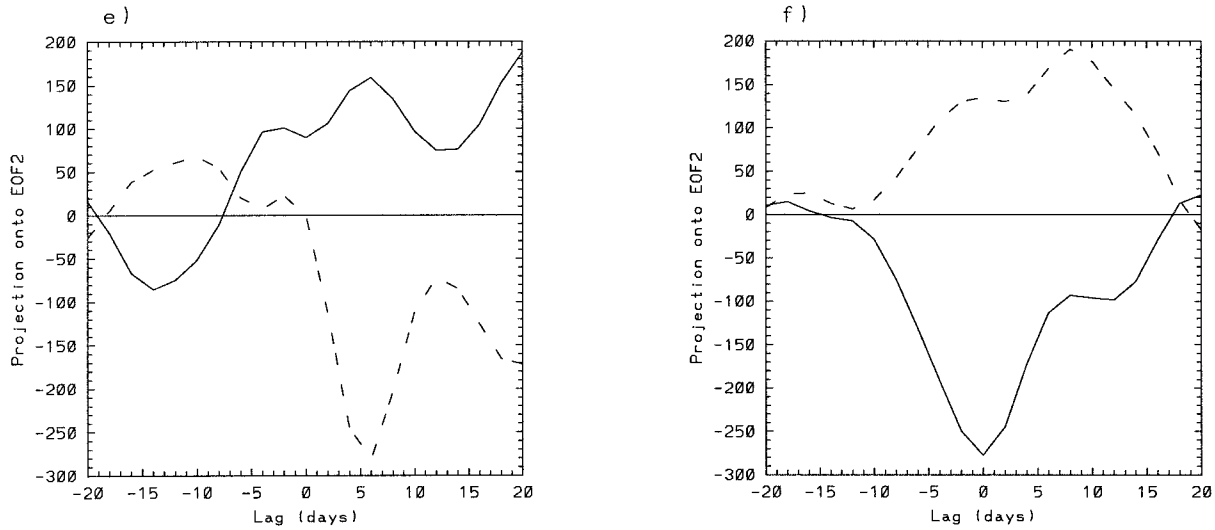

FIG. 5. (*Continued*) tive phase, solid line ξ_3, dashed line $\xi_1 + \xi_2 + \xi_4$.

ming over all N grid points in the Northern Hemisphere yields

$$\frac{da_2}{dt} = \sum_{i=1}^{8} \sum_{j=1}^{N} E_2 \xi_i \cos(\theta). \tag{5}$$

Thus, the projection of various combinations of terms on the rhs of (2) onto E_2 gives the contribution of those terms toward the tendency of the principal component of EOF2.

It is important to note that this projection procedure can only diagnose which terms on the rhs of (2) account for changes in the amplitude of a_2. This technique cannot distinguish between those terms on the rhs of (2) that are of small amplitude and those terms that have a large amplitude but are orthogonal to the EOF. Such large amplitude orthogonal terms can only contribute to the propagation of disturbances. However, since the technique described in section 2 isolates nonpropagating persistent anomalies, any large-amplitude orthogonal terms present must be balanced by additional orthogonal terms of opposite sign. Whether such cancelation does take place can be evaluated by looking at the spatial structure of the various terms on the rhs of (2), as in Fig. 4.

The results from the projections of various combinations of ξ_i onto EOF2 are shown in Fig. 5. Again, extremely similar results to those presented in Fig. 5 are also found if the low-pass filtering of both sides of (2) is neglected, indicating that the results of this study are not sensitive to the application of the low-pass filter. The projection of the sum of the four linear terms plus the low-frequency interaction term, that is, $\Sigma_{i=1}^{5} \xi_i$, onto EOF2 is shown for the positive (negative) phase as the solid line in Fig. 5a (Fig. 5b). Overall, for both phases, it can be see that $\Sigma_{i=1}^{5} \xi_i$ contributes toward both the growth of the anomaly before its maximum and the decay of the anomaly afterward.

The projection of the high-frequency forcing term ξ_6 onto EOF2 is shown as dashed lines in Figs. 5a, b. As can be seen, the ξ_6 projection is of one sign both from a few days before until more than 15 days after onset. This corresponds to the period of time when the low-frequency anomaly is already well established. Also, Figs. 5a and 5b indicate that the ξ_6 projection is much smaller in amplitude than that for $\Sigma_{i=1}^{5} \xi_i$. Furthermore, the projection from $\Sigma_{i=1}^{5} \xi_i$ leads that from ξ_6 by several days. The time sequence for ξ_6, illustrated in Fig. 6, shows that ξ_6 and the positive contribution toward EOF2 closely match after lag -2 days. Although not shown, this match in spatial patterns extends to lag $+14$ days. A similar spatial relationship is found for the negative phase, except that the amplitude of the high-frequency forcing is reduced.

The above behavior suggests that the high-frequency forcing ξ_6 is set up in response to the low-frequency anomaly, rather than ξ_6 actually driving the anomaly. Furthermore, as the similarity in the spatial patterns between ξ_6 and EOF2 extends well beyond the typical lifetime of an individual high-frequency transient eddy, it is likely that a feedback is taking place whereby the high-frequency transients are amplifying the low-frequency anomaly. The extent to which the high-frequency transients directly influence the low-frequency anomaly can be evaluated by comparing the time integral of the principal component tendency time series, that is, da_2/dt, both with and without the high-frequency forcing present. That is, compare the time integral of $\Sigma_{i=1}^{5} \xi_i$ with that for $\Sigma_{i=1}^{6} \xi_i$. This simple calculation finds that ξ_6 influences only the length of the persistent episode, not the maximum anomaly amplitude. For the positive (negative) phase, ξ_6 extends the length of the persistent episode by about one-third (one-tenth). These results imply that the high-frequency eddies play an

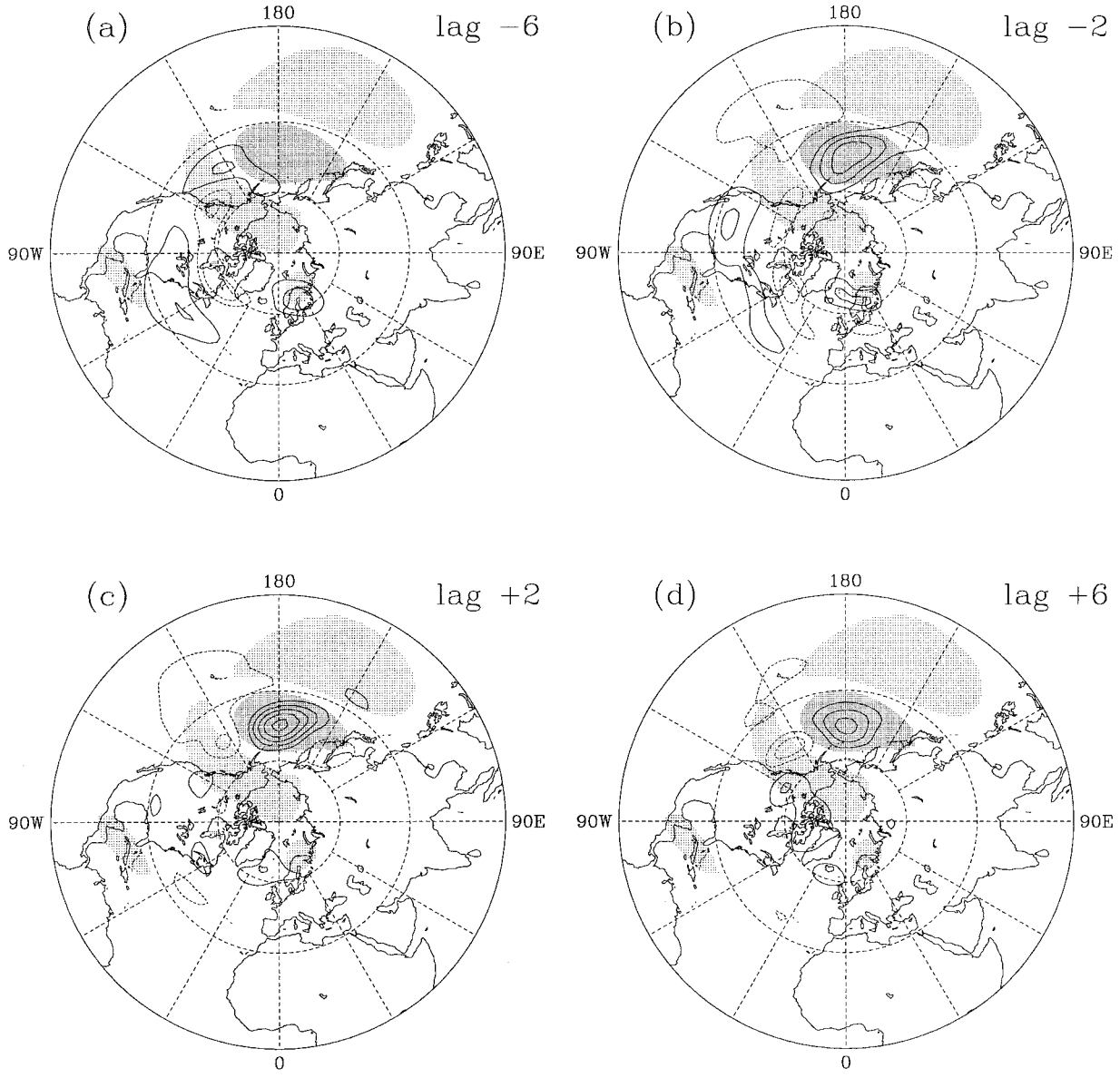

FIG. 6. Composites of the high-frequency forcing term ξ_6 at (a) lag −6 days, (b) lag −2 days, (c) lag +2 days, and (d) lag +6 days. Contour interval is 5.0 $m^2\ s^{-2}$. Solid contours are positive, dashed contours negative, and the zero contour is omitted. Dense (light) stippling indicates positive (negative) values of EOF2. The stippling is above a magnitude of 0.40.

important role in the maintenance of the low-frequency anomaly only for the positive phase.

A calculation of the time average of the projections over the lifetime of the anomaly finds an approximate balance between the $\Sigma_{i=1}^{5}\ \xi_i$ and ξ_6 projections. This balance is to be expected because of the smallness of ξ_7, ξ_8, and the time average of da_2/dt. Such a balance might lead one to the conclusion that the high-frequency transients are maintaining the low-frequency anomaly. This conclusion would be misleading for the positive phase, because $\Sigma_{i=1}^{5}\ \xi_i$ contributes substantially toward the growth of the anomaly, and incorrect for the negative phase. The source of this possible confusion is that time averages do not reveal the large temporal evolution of $\Sigma_{i=1}^{5}\ \xi_i$.

The separate projection for the sum of the four linear terms $\Sigma_{i=1}^{4}\ \xi_i$ and the low-frequency interaction term ξ_5 is illustrated for the positive and negative phases in Figs. 5c and 5d, respectively. Although differences between the two phases are evident, it is clear that the sum of the linear terms, $\Sigma_{i=1}^{4}\ \xi_i$, is usually the dominant contributor to both growth and decay of the anomaly. The primary exception occurs during the anomaly decay for the negative phase, where $\Sigma_{i=1}^{4}\ \xi_i$ and ξ_5 are of similar magnitude. Thus, from the simplest perspective, these results suggests that the anomaly grows and decays *lin-*

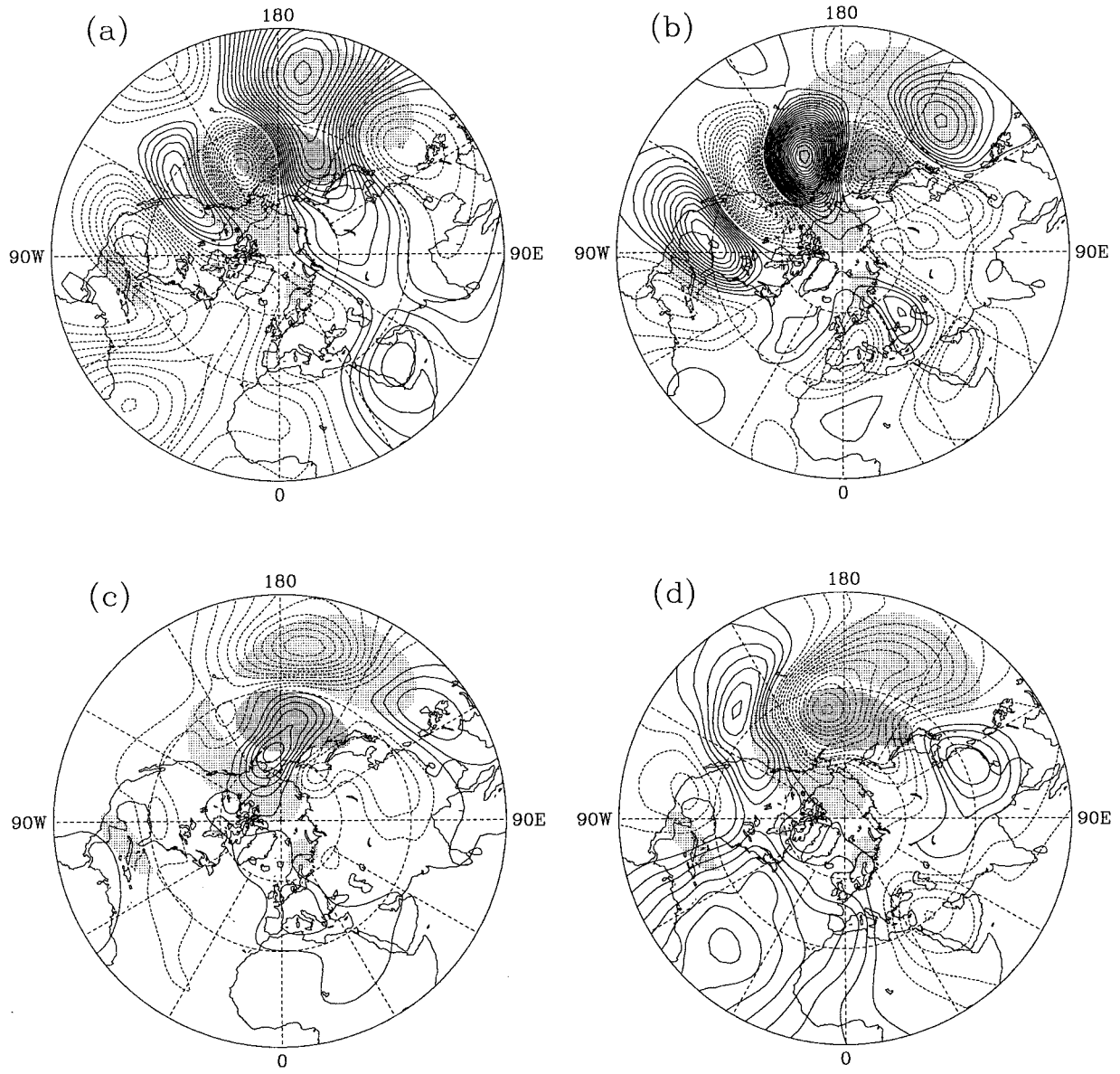

FIG. 7. Composites of (a) ξ_1, (b) ξ_2, (c) ξ_3, (d) ξ_4, at lag +6 days for the positive phase. The contour interval is 10.0 m^2 s^{-2}. Solid contours are positive, dashed contours negative, and the zero contour is omitted. Dense (light) stippling indicates positive (negative) values of EOF2. The stippling is above a magnitude of 0.40.

early, with important contributions from the high-frequency (low frequency) eddies during the decay of the positive (negative) phase.

Further insight into the properties of the linear terms can be obtained by decomposing the projection of the sum of the linear terms into that from ξ_3, the interaction between the low-frequency anomaly and the zonally asymmetric flow, and that from the sum of the three remaining terms, ξ_1, ξ_2, and ξ_4. These projections are shown in Figs. 5e and 5f for the positive and negative phases, respectively. For both phases, it can be seen that ξ_3 amplifies the anomaly both while it is growing and throughout the persistent episode, whereas the sum of the three remaining terms damp the anomaly once it is established. A separate analysis of each of the three remaining terms finds that the divergence term ξ_4 is the main contributor to the anomaly decay. An examination of the spatial structure of each of the linear ξ_i at the time of the maximum projections for both ξ_3 and the sum of the remaining terms reveals interesting characteristics. Compared to lag −2 days (Figs. 4c–f), the changes in ξ_1, ξ_2, ξ_3 (see Figs. 7a–c) are relatively small, the primary alternations being an amplification of ξ_3 and a westward displacement of ξ_1 and ξ_2. On the other hand, the changes in spatial structure of the divergence ξ_4 are dramatic (see Fig. 7d).

The above characteristics for the linear terms, together with the properties for the composite temporal evolution of the low-frequency anomaly, suggest the following picture: As the anomalies propagate westward (Figs. 3a–c), they enter a region of diffluence downstream of the time-mean jet (the jet maxima is located at approximately 30°N, 150°E). Once in this region, the anomalies becomes stationary and amplify via their interaction with the zonally asymmetric time-mean flow. Together with the high-frequency transients (positive phase only), it is this interaction that maintains the anomaly throughout the persistent episode. During this period of amplification, the accompanying modification to the spatial structure of the anomalies (Figs. 3d–f) results in changes in the divergence term that lead to the ultimate decay of the anomaly.

e. Divergence equation

As stated in the introduction, the low-frequency streamfunction anomaly can be implicitly driven via the divergence equation. In particular, within this equation, it is possible for high-frequency transient eddies to directly force a divergence anomaly, which in turn influences the streamfunction anomaly through the divergence term in the vorticity equation. Thus, as with (2), each term in the velocity potential tendency equation (the inverse Laplacian of the divergence equation) was filtered and separated into linear and high- and low-frequency nonlinear components. Given the well-known scaling of the divergence equation for synoptic-scale motions (e.g., Haltiner and Williams 1980), where the divergence tendency is much smaller than several linear and nonlinear terms, the balance was found to be poor. Nevertheless, it was found that the high-frequency forcing term did not project onto either the anomalous velocity potential or its tendency, and for both phases, this forcing term attained its maximum amplitude 4 days after onset. This result suggests that such implicit forcing of the streamfunction anomaly by the high-frequency transient eddies is not taking place.

4. Conclusions

The key result in this study was obtained by projecting composites of various terms in the streamfunction tendency equation onto a particular streamfunction EOF. This EOF is characterized by a wave train confined to the North Pacific. The projection of these terms, which is a measure of their contribution to the tendency of the principal component of the EOF, indicated that at most times the growth and decay of the anomaly was dominated by the sum of the *linear* terms. At other times, especially during the decay of the anomaly, the high- and low-frequency transient eddies made important contributions to the evolution of the anomaly. An examination of the projections of individual linear terms found that the interaction between the low-frequency anomaly and the zonally asymmetric time mean flow (Frederiksen 1983; Simmons et al. 1983) accounted for both the growth and the maintenance of the low-frequency anomaly. The decay of the anomaly was accomplished by the divergence term.

The results of this study also suggest that the high-frequency transients are reorganized by the low-frequency anomaly in such a manner as to project onto the low-frequency anomaly; that is, there is a high-frequency eddy feedback taking place. This reorganization in the structure of the high-frequency transient eddies may simply result from steering and straining by the background low-frequency flow field (e.g., Nakamura and Wallace 1990; Lee 1995; Whitaker and Dole 1995). A close examination of the projection of the high-frequency forcing term showed that although its influence on the low-frequency anomaly was negligible for the negative phase, it did contribute toward a considerable extension of the length of the persistent episode for the positive phase. Thus, this study has presented two extreme cases, one in which the high-frequency eddies contribute to the maintenance of the low-frequency anomaly and the other in which they do not.

Many studies of low-frequency variability examine the maintenance of monthly or seasonally averaged anomalies. The results of this study question this approach because such relatively long time averages might extend beyond the lifetime of the anomaly. Since the time-averaged tendency term is small, a long time average must yield a balance between the linear and nonlinear terms, giving an impression of maintenance of the low-frequency anomaly by high-frequency transients. Such an impression would have been somewhat misleading for the positive phase, since the main contributor to the maintenance of the low-frequency anomaly is the interaction between the low-frequency anomaly and the zonally asymmetric time-mean flow, and incorrect for the negative phase, since the role of the high-frequency transients was found to be negligible for that phase.

The key result of this investigation has been hinted at in other studies of low-frequency variability. For example, Black and Dole (1993) showed that a volume-integrated eddy enstrophy associated with a North Pacific low-frequency anomaly grows primarily by the linear interaction of the anomaly with the time-mean flow. Two other studies, Schubert et al. (1993) and Cai and Van den Dool (1994), examine the contribution from individual terms in the composite vorticity equation toward the maintenance of low-frequency anomalies. Schubert et al. (1993) examine a North Pacific anomaly, and Cai and Van den Dool (1994) investigate zonal wavenumbers 1 through 4. In both studies, at the time of the maximum anomaly, it was found that the linear terms were much larger than the nonlinear terms.

The results of this study do not rule out the possibility that the high-frequency transient eddies can still play an important role in exciting the low-frequency anom-

aly. For example, because the streamfunction tendency budget shows that the linear terms are dominant as the anomaly grows, it is possible that the low-frequency anomaly may be undergoing either modal (e.g., Frederiksen 1983; Simmons et al. 1983) or nonmodal (e.g., Farrell 1989) growth. As shown by Borges and Hartmann (1992), for anomalies that grow on timescales of several days, as in the present study, both modal and nonmodal disturbances exhibit a similar growth rate. If the spatial structure of the high-frequency transient forcing projects onto the adjoint of a rapidly growing unstable normal mode, or it excites one of the fastest growing optimals, the high-frequency transient eddies could indeed trigger low-frequency anomaly evolution. Such a scenario cannot be diagnosed by comparing the magnitude of various terms in a budget analysis, as the relevant high-frequency forcing would take place well before onset, and would probably have a spatial structure very different from the EOF. Another manner in which the high-frequency forcing could be important involves resonance, at least while the low-frequency anomaly is growing. That both the streamfunction tendency and the linear summation are both much larger than the high-frequency forcing is not inconsistent with such a possibility.

An outstanding issue has been whether the dynamics of regional low-frequency anomalies can be interpreted as zonal index dynamics confined to the vicinity of the anomaly. Since the anomalies associated with EOF2 correspond to meridional jet displacements, a key characteristics of the zonal index (Robinson 1991; Yu and Hartmann 1993; Lee and Feldstein 1996; Feldstein and Lee 1996), this question can be addressed from the results of the present study. Because the zonal index is characterized by zonal jet displacements that are driven by high-frequency transient eddies, rather than the high-frequency transient eddies responding to the presence of the low-frequency anomaly, as shown in this study for EOF2, the regional low-frequency anomaly examined in this paper cannot be understood as exhibiting zonal index behavior.

Acknowledgments. I would like to thank Dr. Sukyoung Lee for her beneficial discussions on this subject and her comments on this manuscript. I would also like to thank two anonymous reviewers whose comments improved this manuscript. This research was supported by the National Science Foundation through Grant ATM-9416701.

REFERENCES

Barnston, A. G., and R. E. Livezey, 1987: Classification, seasonality, and persistence of low-frequency atmospheric circulation patterns. *Mon. Wea. Rev.,* **115,** 1083–1126.

Black, R. X., and R. M. Dole, 1993: The dynamics of large-scale cyclogenesis over the North Pacific Ocean. *J. Atmos. Sci.,* **50,** 421–442.

Borges, M. D., and D. L. Hartmann, 1992: Barotropic instability and optimal perturbations of observed nonzonal flows. *J. Atmos. Sci.,* **49,** 335–354.

Branstator, G., 1984: The relationship between the zonal mean flow and quasi-stationary waves in the midtroposphere. *J. Atmos. Sci.,* **41,** 2163–2178.

——, 1990: Low-frequency patterns induced by stationary waves. *J. Atmos. Sci.,* **47,** 629–648.

——, 1992: The maintenance of low-frequency atmospheric anomalies. *J. Atmos. Sci.,* **49,** 1924–1945.

Cai, M., and H. M. van den Dool, 1994: Dynamical decomposition of low-frequency tendencies. *J. Atmos. Sci.,* **51,** 2086–2100.

Dole, R. M., 1986: The life cycles of persistent anomalies and blocking over the North Pacific. *Advances in Geophysics,* Vol. 29, Academic Press, 31–69.

——, and R. X. Black, 1990: Life cycles of persistent anomalies. Part II: The development of persistent negative height anomalies over the North Pacific Ocean. *Mon. Wea. Rev.,* **118,** 824–846.

Egger, J., and H.-D. Schilling, 1983: On the theory of the long-term variability of the atmosphere. *J. Atmos. Sci.,* **40,** 1073–1085.

Farrell, B. F., 1989: Optimal excitation of baroclinic waves. *J. Atmos. Sci.,* **46,** 1193–1206.

Feldstein, S. B., and S. Lee, 1996: Mechanisms of zonal index variability in an aquaplanet GCM. *J. Atmos. Sci.,* **53,** 3541–3555.

Frederiksen, J. S., 1983: A unified three-dimensional instability theory of the onset of blocking and cyclogenesis. II: Teleconnection patterns. *J. Atmos. Sci.,* **40,** 2593–2609.

Gordon, C. T., and W. T. Stern, 1982: A description of the GFDL global spectral model. *Mon. Wea. Rev.,* **110,** 625–644.

Haltiner, G. J., and R. T. Williams, 1980: *Numerical Prediction and Dynamic Meteorology.* Wiley and Sons, 477 pp.

Hansen, A. T., and A. Sutera, 1995: Large amplitude flow anomalies in the Northern Hemisphere midlatitudes. *J. Atmos. Sci.,* **52,** 2133–2151.

Higgins, R. W., and S. D. Schubert, 1994: Simulated life cycles of persistent anticyclonic anomalies over the North Pacific: Role of synoptic-scale eddies. *J. Atmos. Sci.,* **51,** 3238–3260.

——, and ——, 1996: Simulations of persistent North Pacific circulation anomalies and interhemispheric teleconnections. *J. Atmos. Sci.,* **53,** 188–207.

Horel, J. D., 1985: Persistence of the 500-mb height field during Northern Hemisphere winter. *Mon. Wea. Rev.,* **113,** 2030–2042.

Hoskins, B. J., and D. Karoly, 1981: The steady linear response of a spherical atmosphere to thermal and orographic forcing. *J. Atmos. Sci.,* **38,** 1179–1196.

——, I. N. James, and G. H. White, 1983: The shape, propagation and mean-flow interaction of large-scale weather systems. *J. Atmos. Sci.,* **40,** 1595–1612.

Kang, I.-S., 1990: Influence of zonal mean flow change on stationary wave fluctuations. *J. Atmos. Sci.,* **47,** 141–147.

——, and K.-M. Lau, 1994: Principal modes of atmospheric circulation anomalies associated with global angular momentum fluctuations. *J. Atmos. Sci.,* **51,** 1194–1205.

Lau, N.-C., 1988: Variability of the observed midlatitude storm tracks in relation to low-frequency changes in the circulation pattern. *J. Atmos. Sci.,* **45,** 2718–2743.

Lee, S., 1995: Localized storm tracks in the absence of local instability. *J. Atmos. Sci.,* **52,** 977–989.

——, and S. B. Feldstein, 1996: Mechanisms of zonal index evolution in a two layer model. *J. Atmos. Sci.,* **53,** 2232–2246.

Mo, K. C., 1986: Quasi-stationary states in the Southern Hemisphere. *Mon. Wea. Rev.,* **114,** 808–823.

Nakamura, H., and J. M. Wallace, 1990: Observed changes in baroclinic wave activity during the life cycles of low-frequency circulation anomalies. *J. Atmos. Sci.,* **47,** 1100–1116.

Navarra, A., and K. Miyakoda, 1988: Anomaly general circulation models. *J. Atmos. Sci.,* **45,** 1509–1530.

Nigam, S., and R. S. Lindzen, 1989: The sensitivity of stationary waves to variations in the basic state zonal flow. *J. Atmos. Sci.,* **46,** 1746–1768.

North, G. R., T. L. Bell, R. F. Cahalan, and F. J. Moeng, 1982. Sam-

pling errors in the estimation of empirical orthogonal functions. *Mon. Wea. Rev.,* **110,** 699–706.

Robinson, W., 1991: The dynamics of the zonal index in a simple model of the atmosphere. *Tellus,* **43A,** 295–305.

Schubert, S. D., and C.-K. Park, 1991: Low-frequency intraseasonal tropical–extratropical interactions. *J. Atmos. Sci.,* **48,** 629–650.

——, M. Suarez, C.-K. Park, and S. Moorthi, 1993: GCM simulations of intraseasonal variability in the Pacific/North American region. *J. Atmos. Sci.,* **50,** 1991–2007.

Simmons, A. J., J. M. Wallace, and G. Branstator, 1983: Barotropic wave propagation and instability and atmospheric teleconnection patterns. *J. Atmos. Sci.,* **40,** 1363–1392.

Ting, M., and N.-C. Lau, 1993: A diagnostic and modeling study of the monthly mean wintertime anomalies appearing in an 100-year GCM experiment. *J. Atmos. Sci.,* **50,** 2845–2867.

Wallace, J. M., and D. S. Gutzler, 1981: Teleconnections in the geopotential height field during the Northern Hemisphere winter. *Mon. Wea. Rev.,* **109,** 784–812.

Whitaker, J. S., and R. M. Dole, 1995: Organization of storm tracks in zonally varying flows. *J. Atmos. Sci.,* **52,** 1178–1191.

Yang, S., and B. Reinhold, 1991: How does the low-frequency variance vary? *Mon. Wea. Rev.,* **119,** 119–127.

Yu, J.-Y., and D. L. Hartmann, 1993: Zonal flow vacillation and eddy forcing in a simple GCM of the atmosphere. *J. Atmos. Sci.,* **50,** 3244–3259.